Growth Quantification and Length Distributions of DNA Origami Polymers

Undergraduate Honors Thesis

For Partial Fulfillment of Requirements to Graduate with Honors Research Distinction

Clinton LeHotan

Advisor: Dr. Carlos Castro

3/29/2013

Abstract

DNA origami is a new technology that uses DNA to create nanoscale engineered structures via molecular assembly. DNA origami structures have been developed for a wide range of useful applications including studying different aspects of biomolecular systems, substrates for single molecule reactions (Jungmann, Scheible et al. 2011), and even as a potential cancer drug delivery system (Zhao, Shaw et al. 2012). Since many biological systems, in particular cellular systems, are on the order of microns in length, larger DNA origami structures are required for analysis. One method that can be used to create larger DNA origami structures is called polymerization. The polymerization process bonds DNA origami monomers, individual structures, together in one dimensional arrays, termed filaments, by using small sections of ssDNA that protrude from monomer ends to function as sticky-ends for larger scale assembly. To better understand the method of polymerization, the filament assembly process was analyzed as a function of time using Transmission Electron Microscopy (TEM). The data shows that as the average length of the polymer increases with a typical timescale to achieve micron scale filaments of around 6 hours with a limiting factor of the monomer concentration is indicated by depletion of monomers. Since the TEM uses a negative staining process, which fixes the DNA origami structures into static configurations, fluorescence microscopy was investigated as a possible medium to view the polymerization of DNA origami structures in real time.

Acknowledgements

I would like to thank Dr. Carlos Castro for all of his help and support throughout the entire research process. He provided excellent leadership and was an asset into the fields of biology, biochemistry, and DNA origami. Dr. Castro was always willing to meet to discuss problems that I was having with the research, no matter the time or place. Since I did not have an intensive background in biology, he was always there to explain the different characteristics of DNA.

Along with Dr. Castro, I would like to thank Dr. Rob Siston for his help with the honors undergraduate research class and in preparation for this defense. I have learned a substantial amount about presentations and I have truly grown through the class.

I would also like to thank Danny Turowski who was a big help with the folding, polymerization, and purification of DNA origami structures. It was very nice to be able to work with someone who is understanding and is always willing to teach. His previous work on polymerization was vital in helping speed up the design process for my flat 18 helix bundle design.

Finally, I would like to thank all of the members of the Nanoengineering and Biodesign Lab (NBL). Everyone in the lab accepted me into their group with open arms and I was able to make many new friends throughout the process.

Table of Contents

List of Figures

List of Tables

Chapter 1: Introduction and Background

DNA Background

Deoxyribonucleic Acid, or DNA, which contains the genetic code for all living things, is comprised of purine and pyrimidine nucleotide bases that are bonded to a backbone of phosphate and sugar (Nelson and Cox 2008). The purine bases consist of adenine, A, and guanine, G, and the pyrimidine bases include cytosine, C, and thymine, T. Single-stranded DNA, ssDNA, consists of a string of nucleotide bases attached to the phosphate-sugar backbone. Double-stranded DNA, dsDNA, consists of two strands of ssDNA that are bonded together into a double helical configuration via hydrogen bonds that form between nucleotide bases of opposing strands. These bases bond together in pairs with adenine binding only to thymine and guanine binding only with cytosine. This specific bonding between nucleotides is called Watson-Crick base pairing.

Double-stranded DNA can be melted into its single-stranded components by heating. This process as described by Nelson and Cox (Nelson and Cox 2008) involves melting, or denaturation, which is the separation of DNA into individual strands by heating. The high temperature causes the hydrogen bonds between the bases to destabilize and ultimately break, thereby separating the DNA into two complementary strands. By cooling the single strands of DNA, the hydrogen bonds will reform and the two strands will self-assemble into the original double helical configuration. DNA from different sources can be annealed together in a process called hybridization. If the bases of each strand are complimentary, then when annealed, they will form what are called hybrid duplexes. Hybrid duplexes are comprised of two separate strands of ssDNA that are annealed together by base-pairing interactions. The melting and

annealing temperatures of double-stranded DNA are dependent on the sequence and length. Typical melting/annealing temperatures for strands used in DNA origami vary from 30-70^{o}C.

DNA Origami Introduction

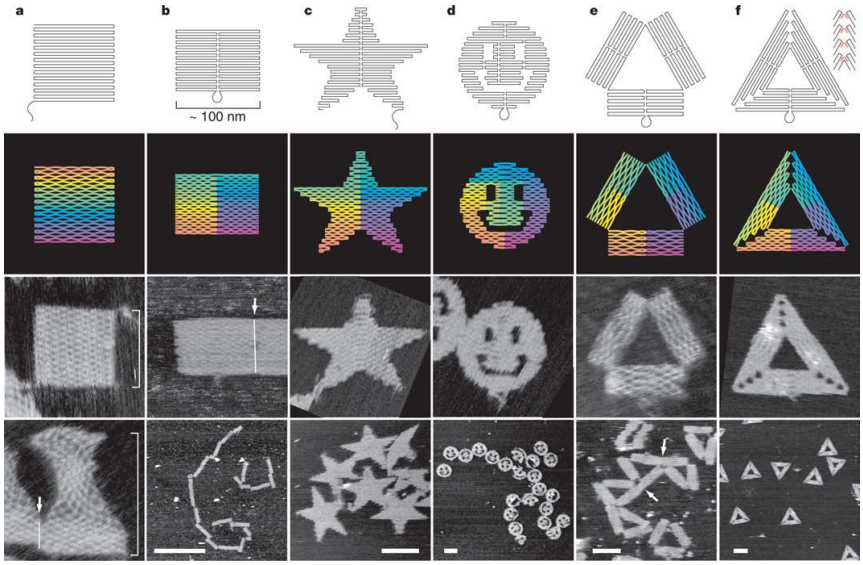

Figure 1: Example of DNA Origami Structures (Rothemund 2006)

DNA origami is a recently developed technology that exploits the molecular self-assembly characteristics of DNA to create nanoscale engineered structures (Castro, Kilchherr et al. 2011) (Rothemund 2006). The individual DNA origami structures typically range from approximately 50nm to 400nm in length, depending on the cross sectional geometry of the structure. Figure 1 shows some of the first structures that were created using this technology (Rothemund 2006).

DNA origami structures are created using a long single-stranded “scaffold” and many short single-stranded “staples” (Castro, Kilchherr et al. 2011). At any position in a DNA origami structure, one strand in the double-helix is contributed by the scaffold strand, which is a long circular piece of genomic DNA derived from the M13MP18 bacteriophage virus. The scaffold is

around 7000-8000 bases in length and has a sequence that is fully known. The staple strands are much shorter, 30-50 bases in length, and are designed to be piecewise complimentary to sections of the scaffold strand that may be distant along the primary base sequence. During self-assembly, the scaffold must fold in order to spatially collocate sections of the scaffold that bind to a single staple. Hence, the staple sequences determine the scaffold folding pattern. This manipulation "programs" the DNA to fold into a pre-designed geometry. Figure 2 illustrates the basic folding process for creating DNA origami structures with a scaffold strand and two staple strands. Typically structures comprise of 150-200 staple strands.

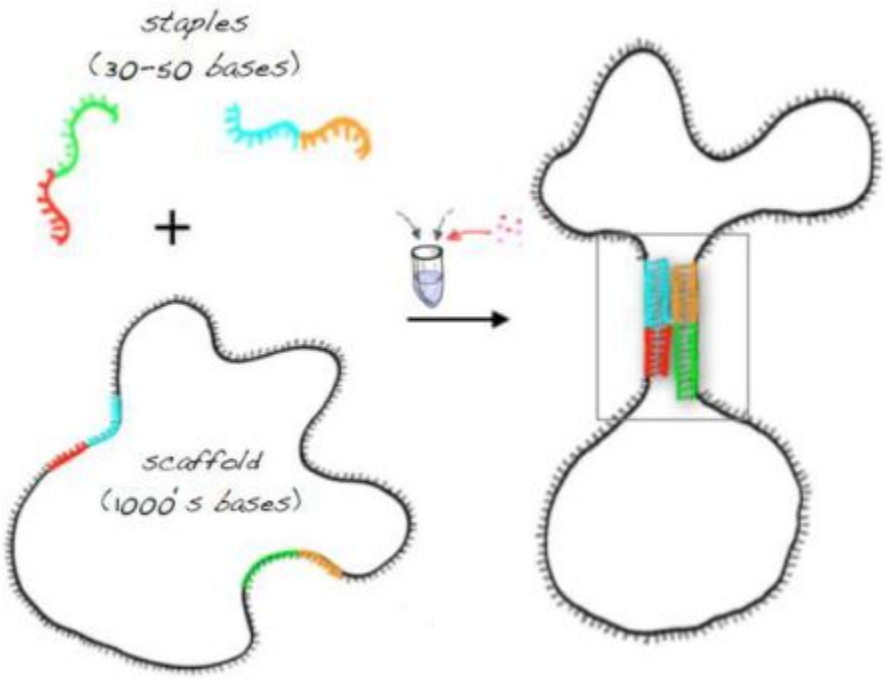

Figure 2: Image Courtesy of Hendrik Deitz

DNA origami nanostructures have also been developed for applications including templates for single molecule reactions, tracks for molecular walkers (Jungmann, Scheible et al.

2011), and nanopores for single molecule sensing (Langecker, Arnaut et al. 2012). Researchers are even looking towards DNA origami as a new type of specialized cancer drug delivery system (Zhao, Shaw et al. 2012). The Nanoengineering and Biodesign Lab (NBL) at The Ohio State University uses DNA origami as a tool to study biological and cellular systems.

Process for Creating DNA Origami Structures

DNA origami is a "bottom-up" approach to design and fabrication (Rothemund 2006). The first step of the design process is to determine the desired structure geometry. In DNA origami structural design, the naturally occurring DNA double helix is normally depicted as a cylinder (Castro, Kilchherr et al. 2011). Once the target structure has been conceptualized, the second step of the design process is to approximate your desired geometry as a group of cylinders as shown in Figure 3. Each cylinder, which represents a dsDNA helix, has a diameter of ~2 nm and a length that is tunable according to the number of base-pairs placed in a helix. The length of dsDNA is .334 nm/bp.

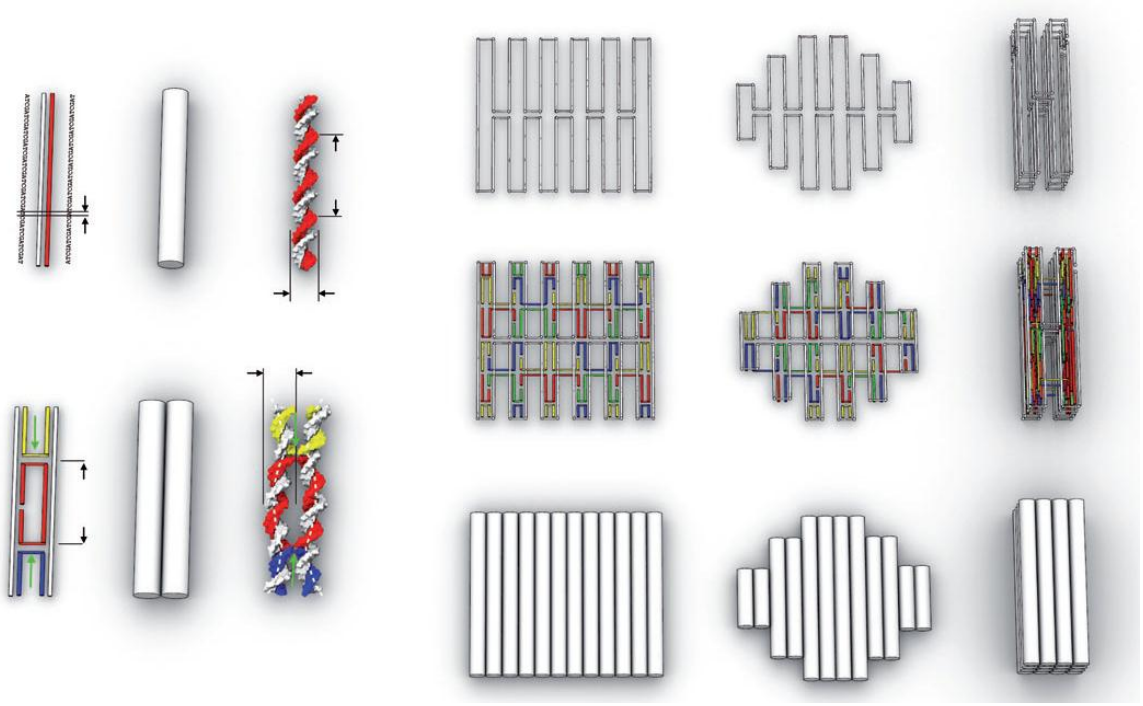

Figure 3: Depiction of Cylindrical Approximations for Double-Stranded DNA Origami Structures (Castro, Kilchherr et al. 2011)

After creating raft-like approximations of the overall design with cylinders, the single scaffold can be routed throughout the entire structure. Since the scaffold is one continuous piece of ssDNA, it must be visit every point on the structure while forming a closed loop.

Staples are then added in with the scaffold making sure to place an adequate number of cross-overs between any two neighboring helices in the design. Crossovers, also known as Holliday junctions, occur when a staple crosses from one helix to a neighboring helix (Castro, Kilchherr et al. 2011). These cross-overs hold the cylinders (DNA helices) together in a predetermined fashion as shown in Figure 3. Next, the staples can be sequenced to determine the assigned base (A, T, G, or C) according to its complementarity to the scaffold. The design process can be expedited by using the computer aided design software caDNAno (Douglas, Dietz

et al. 2009). CaDNAno is a 2D and 3D modeling software that allows for the rapid design of structures and has the ability to automate the sequence design process once the scaffold and staple routing is determined. Figure 4 shows an example of what a caDNAno model looks like where the blue lines represent the scaffold strand and the other colors represent different staple groups. The vertical lines indicate a cross-over between helices.

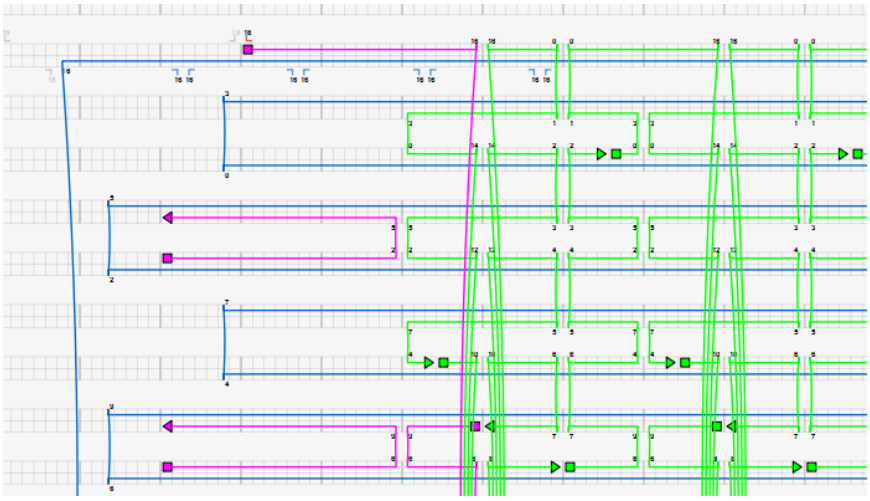

Figure 4: Example of a caDNAno 2-D Model with Scaffold and Staples

The ingredients required to fabricate DNA origami structures include scaffold, staples in excess (usually 10X staples compared to the scaffold), and salt containing buffer (Castro, Kilchherr et al. 2011). Positive ions from the salt are necessary for the folding reactions to screen the electrostatic repulsions of the negatively charged DNA. The folding ingredients are mixed in a self-assembly reaction containing 10-20 nM scaffold, 10x excess of staples compared to the scaffold, 5 mM NaCl, 5 mM Tris Base, 1 mM EDTA, and a $MgCl^2$ concentration ranging from 10-20 mM. Optimal $MgCl^2$ concentrations are determined by screening this range and evaluating folding results. The final folding reaction is subjected to a thermal ramp consisting of a high

temperature phase, around 80˚C, to melt all of the interactions so all DNA is single-stranded. Over the course of a couple of days, the staples are annealed to the scaffold by slowly cooling the structure, thereby folding the DNA into the desired structure. Folding results are generally highly sensitive to salt concentrations. Several different folding reactions at differing salt ($MgCl^2$) concentrations are typically run as a screen to determine the optimal folding conditions.

Once the thermal ramp is complete, a process called agarose gel electrophoresis is used to purify the folded structures. The purification step is required to isolate well-folded structures from any misfolded structures and remove excess staples that did not bind to any scaffold. After the thermal ramp, folded samples are pipetted in the wells shown at the left of Figure 5. A voltage (70V) is applied across the gel. The negatively charged DNA will travel through the gel towards the positive end, in this case towards the right end. Since the unbound staples are the smallest structures present in the folding reaction, they run the fastest (blue box in Figure 5). Scaffolds that have folded into the proper structure are more compact than misfolded structures, and hence form a bright narrow band as shown at the right end of the red box in Figure 5. The well-folded structures can then be cut out of the gel and removed from the agarose gel by filtration. In this case the folding results were relatively insensitive to the $MgCl^2$ concentration. The Gel in Figure 5 shows where structures at different magnesium concentrations. The green box indicates the scaffold that is run to verify its integrity.

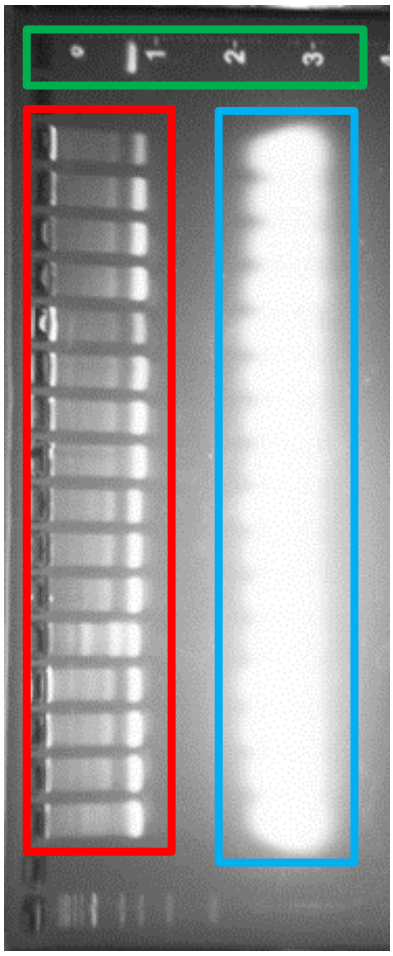

Figure 5: Sample Aragose Gel Image of Flat 18 Helix Bundle Structure. Red box represents the monomers at different magnesium concentrations, blue box shows excess staples, and the green box shows the scaffold.

After the structures have been purified, then are imaged by transmission electron microscopy (TEM) as described Castro et al. (Castro, Kilchherr et al. 2011). Figure 6 shows the step-by-step process for the design, fabrication, and analysis of DNA origami structures.

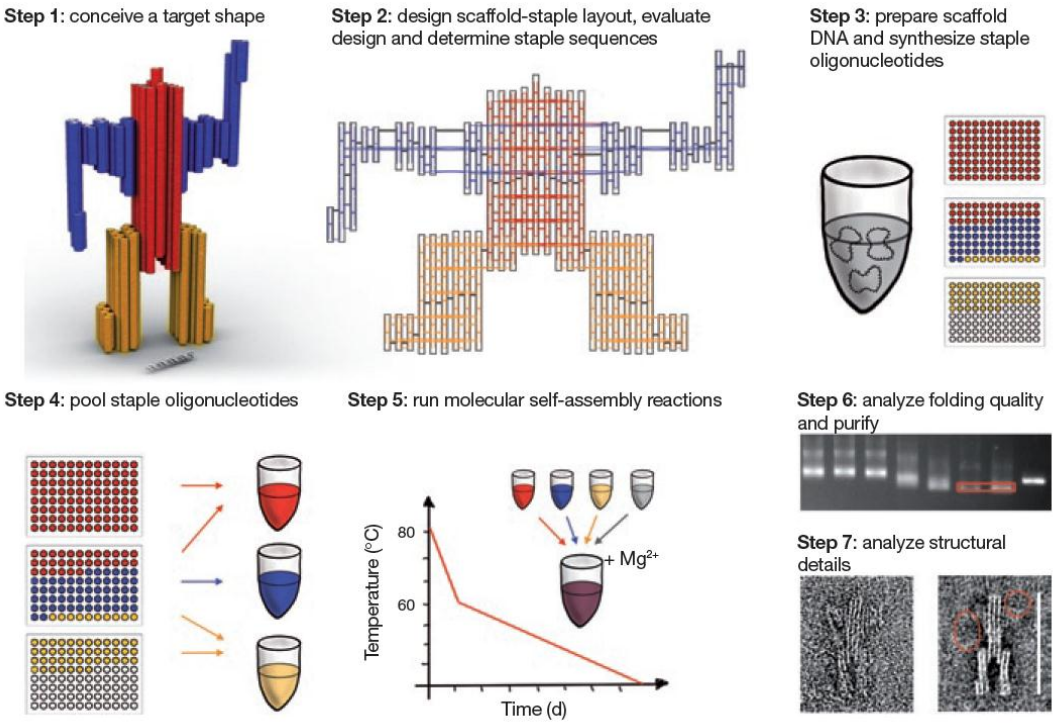

Figure 6: Breakdown of DNA Origami Design, Fabrication, and Analysis (Castro, Kilchherr et al. 2011)

Current Limitations of DNA Origami Structures

The size of a single DNA origami structure is limited by the length of the scaffold since scaffold has to travel throughout the entire structure (Jungmann, Scheible et al. 2011). With the commonly used scaffolds in the 7000-8000 base regime, this yields structures with lengths scales from around 400 nm (small cross sectional area, long structures) to >100 nm (large cross sectional area, short structures). When compared to the average size of a cell, which is around 10 µm, individual DNA origami structures are orders of magnitude smaller. In many cases, in particular for cellular or materials applications, it would be highly useful to be able to scale the functionality of DNA origami structures up to larger dimensions, ideally 1-100µm. This can be achieved by attaching individual structures (monomers) together to create a larger scale

structure. If the attachment is done along a single dimension, this process creates a DNA origami filament, or polymer.

Introduction into Polymerization

Polymerization is the process of connecting smaller structures together to form larger overall structures. Individual DNA origami structures can be designed with open ssDNA bonding sites on the ends of each structure termed "sticky ends." These open bonding sites allow for staples to bridge the gap between different monomers, therefore binding them together to form a larger polymer, or filament. The more monomers that assemble together the longer the filament will be.

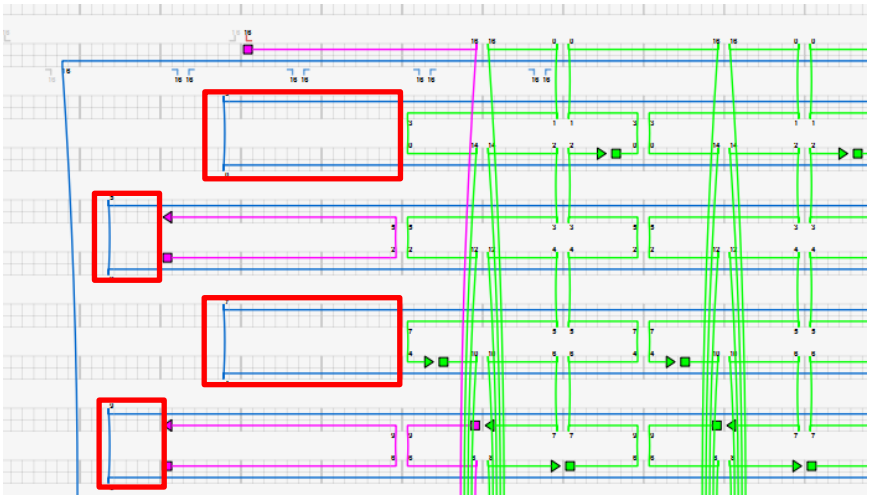

Figure 7: caDNAno Model with Sticky Ends in Red Boxes

This process has been used to create micron-scale filaments (Jungmann, Scheible et al. 2011); however the dynamics of filament grown and the parameters affecting final length are poorly understood. There are limitations with this sticky-end polymerization process. There is essentially no control over the length of the polymers and geometry of the structures since they

are unconstrained in solution. There are also instances of a phenomenon called “branching” which occurs when monomers do not assemble properly leading to geometric discontinuities. Long filaments also tend to entangle in solution making it difficult to distinguish between them or isolate single long filaments.

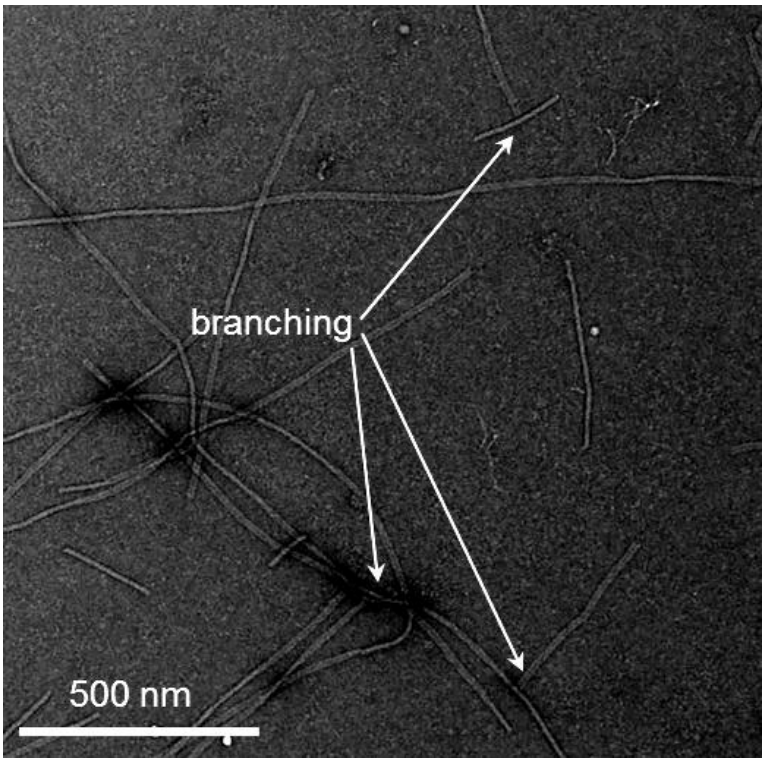

Figure 8: DNA Origami Filaments with Branching (Image Courtesy of Carlos Castro)

Thesis Objectives

The objectives of this thesis are to quantify the polymerization of DNA origami polymers, gather length distribution data for the polymerization process, and design a new DNA origami structure with the ability to analyze different polymerization staple design conditions.

Chapter 2: Structure Design

Monomer Designs

Two monomer designs with distinct cross sectional geometries and overall lengths were analyzed. The first design was created by Danny Turowski which features a hexagonal arrangement of DNA double helices called the “6 helix bundle” (Turowski 2012).

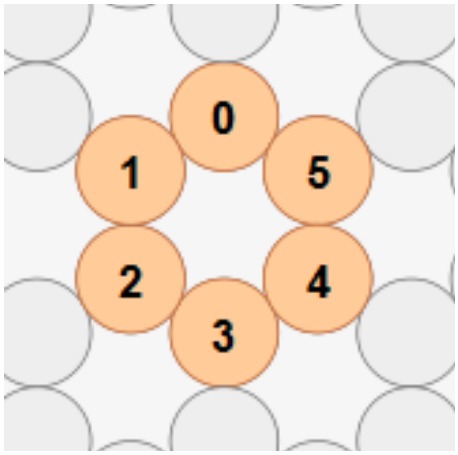

Figure 9: caDNAno Cross Section of 6 Helix Bundle Structure

Figure 9 shows the cross section of the 6 helix bundle where each numbered circle represents a double helix of DNA. Due to the small cross sectional area, the theoretical length of the 6 helix bundle monomer is around 401.9 nm using a scaffold 7560 bases in length (Turowski 2012).

Due to its small cross-sectional geometry, the 6 helix bundle contains only six possible bonding sites (one per helix) to bridge individual monomers. Theoretically, if there are more bonds between the monomers, the filament joints should become more rigid. This addition would increase the stiffness in the joints between monomers. Furthermore the 6 helix bundle has a relatively low bending stiffness because of its small cross-sectional dimensions. This aspect of the design allows the filaments to tangle into tight clumps, rather than form straight, stiff

filaments. The rotational symmetry of the 6 helix bundle monomer also presents challenges with identifying if the filament is twisting about its long axis. If a structure twists about its central axis, then the overall length of the structure may decrease. Finally, the cross sectional area of the 6 helix bundle is small, therefore there is not enough room to add multiple fluorescently labeled staples without encountering interference. Fluorescent molecules that are separated by less than ~10nm are subject to potential self-quenching. In order to address some of the issues with the 6 helix bundle, a new monomer design was created.

Flat 18 Helix Bundle Design

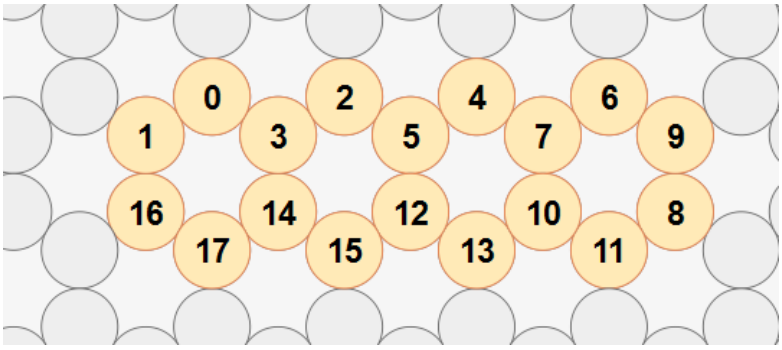

Figure 10: caDNAno Cross Section of Flat 18 Helix Bundle Structure

The new design deemed the "flat 18 helix bundle," with the cross section depicted in Figure 10, is a raft-like structure using similar hexagonal architecture to the 6 helix bundle; however, this design was expanded along the width to create a non-symmetric cross section. By increasing the number of helices in the bundle, the theoretical length of the structure decreases and in this case was found to be around 132 nm with an 8064 base long scaffold. When imaged under a microscope, the new structure should appear in two distinct configurations; horizontal and vertical. The horizontal configuration shows the structure lying flat on four of the double

helices located on the bottom of the structure, where the vertical configuration will have the structure on its edge as shown in Figure 11.

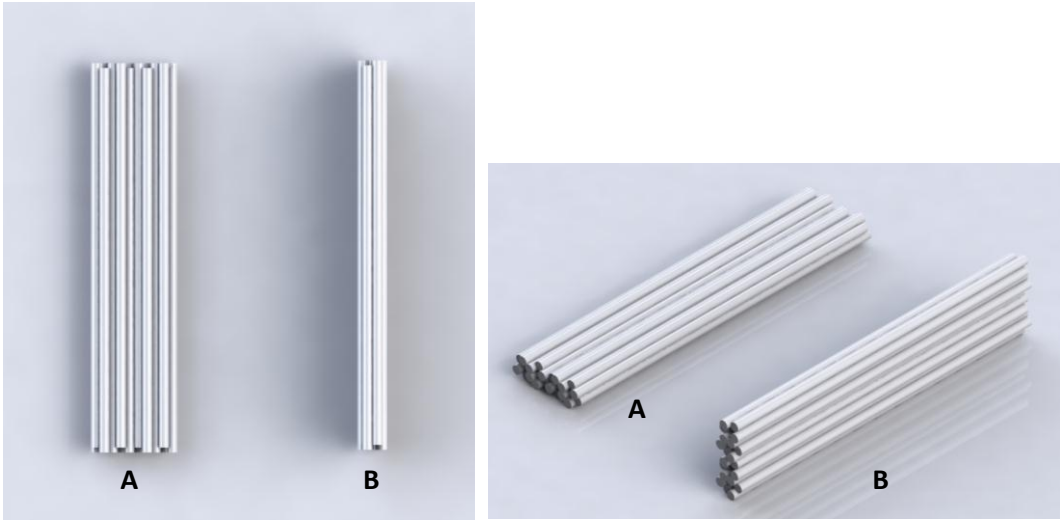

Figure 11: A) Flat 18 Helix Bundle Horizontal Configuration B) Flat 18 Helix Bundle Vertical Configuration

This aspect of the design will be enable direct imaging of any twist that may occur in filaments made from the flat 18 helix bundle under the microscope. The large width of the cross section for the new design also provides enough room for the addition of multiple fluorescently labeled staples. The new design was created in caDNAno and the scaffold and staple routing are shown as a 3D model and a 2D schematic in Figure 12 and Figure 13 respectively.

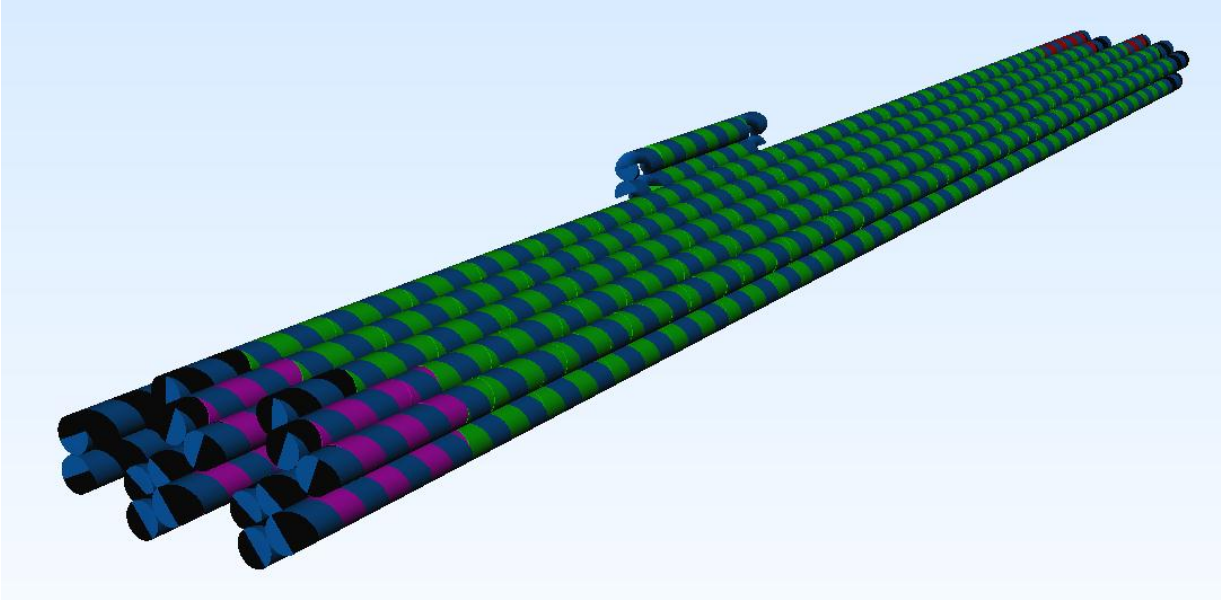

Figure 12: Autodesk Maya Rendering of Flat 18 Helix Bundle caDNAno Model

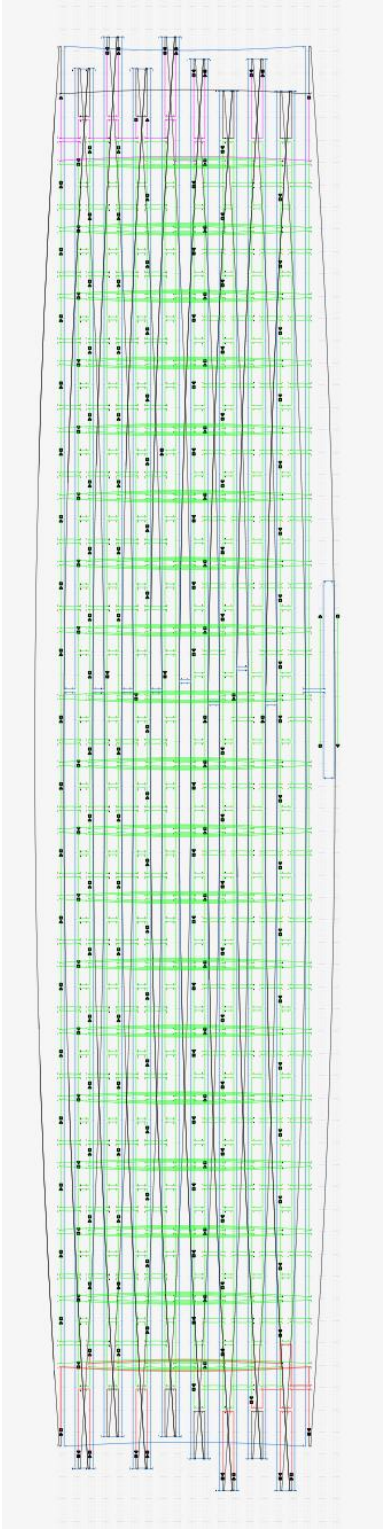

Figure 13: 2-D caDNAno Scaffold and Staple Routing for Flat 18 Helix Bundle with Polymerization Staples

Design of Flat 18 Helix Bundle Polymerization Staples

Currently the design of polymerization staples has not been widely studied. In an attempt to improve the geometric precision of filament assembly as well as increase monomer-to-monomer bond strength, four different designs were created. The design variables we chose to explore include the length of the polymerization toehold on the scaffold as well as the staple crossovers of the monomer staples neighboring the sticky ends. These variables were chosen because we suspect that they may play a major role in the kinetics of polymerization, the overall length achieved, and the mechanical stability of the filaments. Table 1 shows the design matrix for the flat 18 Helix Bundle variations. Figure 14 through Figure 17 show the staple routing for Designs 1 through 4.

Table 1: Design Matrix for Flat 18 Helix Bundle

Design Number	Description
Design 1	Closed neighbor staple configuration with 5 base polymerization staple overlap
Design 2	Open neighbor staple configuration with 5 base polymerization staple overlap
Design 3	Open neighbor staple configuration with 8 base polymerization staple overlap
Design 4	Open neighbor staple configuration with 11 base polymerization staple overlap

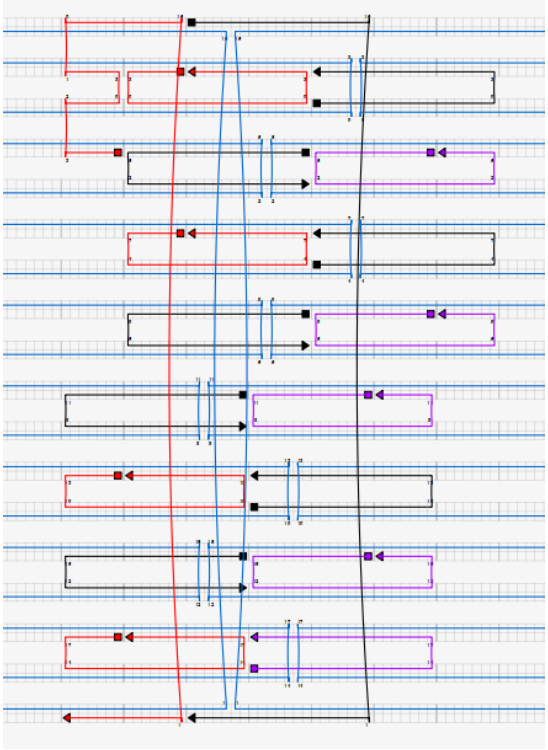

Figure 14: Flat 18 Helix Bundle Design 1

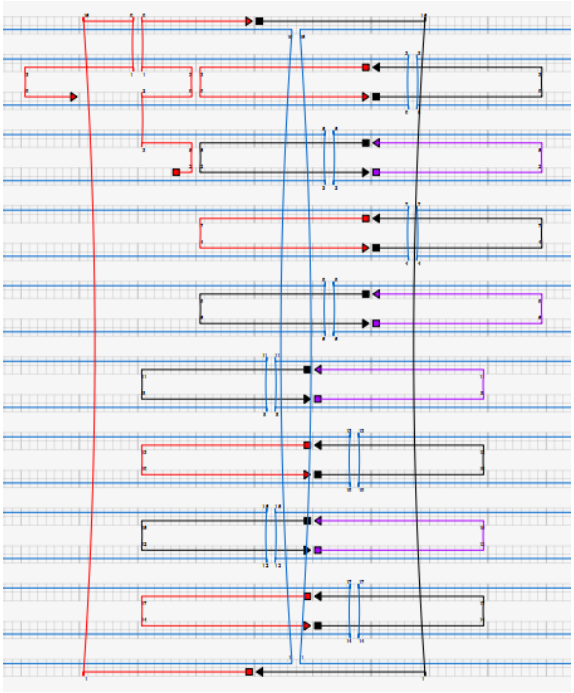

Figure 15: Flat 18 Helix Bundle Design 2

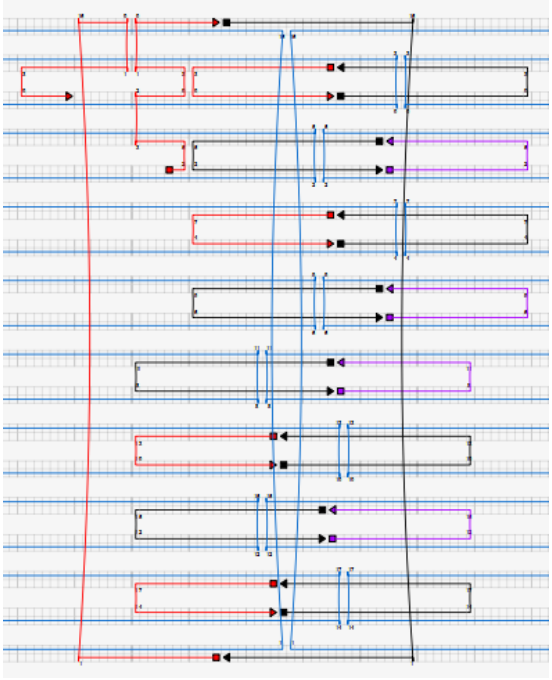

Figure 16: Flat 18 Helix Bundle Design 3

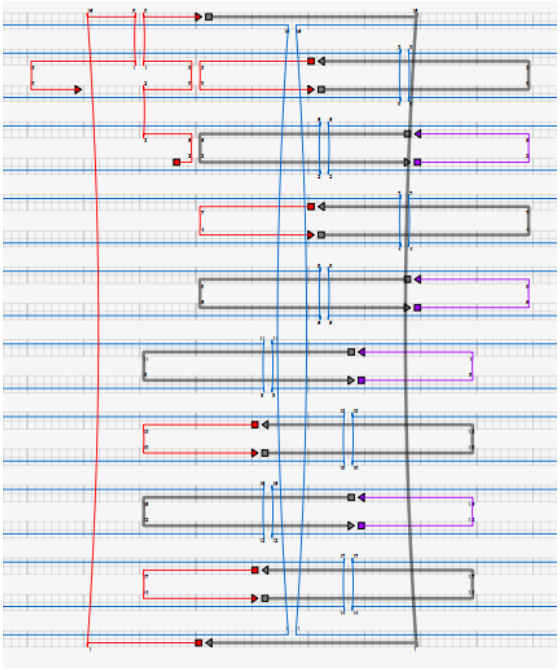

Figure 17: Flat 18 Helix Bundle Design 4

Designs 1 and 2 feature the same five base long sticky ends on the open section, where there is staple no cross over, of the polymerization staples. The difference between the first two designs is in the routing of the staples that are directly next to the polymerization staples. We have termed these staples the “neighboring” staples. Design 1 features a staple cross over at the end of each double helix that neighbors an open polymerization staple. Design 2 does not have staple cross overs at the given locations in Design 1. We suspect that placing a cross-over directly at the binding site of the polymerization staple may constrain the binding of the polymerization staple, which may slow the polymerization; however, the additional cross-over may enhance the local mechanical stability. Design 3 follows the same open neighboring staple configuration as Design 2 with the sticky ends extended by three bases. The final design, Design 4, increases the sticky end length of Design 3 by another three bases, therefore making the total length of the sticky ends 11 bases. When designing polymerization staples, it is desirable to bias the binding to one side of the interface to avoid the situation where polymerization staples occupy both sides of the interface and preclude binding of monomers. Extending the length of these sticky ends will increase the binding affinity, and hence might speed up the assembly time. However, this would also increase the chances that polymerization staples would occupy both sides of the interface. We aim to find the optimal length of sticky ends to balance these competing effects.

Chapter 3: Monomer Self-Assembly and Polymerization

Experimental Design

Experiments were designed to quantify the growth of the DNA origami polymers for the 6 helix bundle and flat 18 helix bundle. The individual monomers were first folded by molecular self-assembly. Once the folding reactions were complete, the purified structures were then polymerized. To be able to view different time points during the polymerization process, polymerization experiments were run at 3, 6, 9, and 24 hours. Transmission Electron Microscopy, or TEM, was then used to analyze the samples. A Matlab script was used to quantify the lengths of the individual monomers and filaments for each sample for further analysis.

Monomer Folding Reactions

The process for folding the monomers follows the procedure outlined by Castro et al (Castro, Kilchherr et al. 2011). 10 µL of 100 nM scaffold and 20 µL of 500 nM staples were added to a 200 µL eppendorff tube. Using an excess of staples increases the likelihood that all of the scaffold strands will be fully populated with staples. 5 µL of 10x FOBXM, which contains 50 mM TRIS, 50 mM NaCl and 10 mM EDTA, was then mixed in with the scaffold and staples, followed by 5 µL MgCl2 concentrations from 12 to 16 mM. Finally, 10 µL of double-distilled water (ddH2O) was added to make a final reaction volume of 50 µL. Since DNA is inherently negatively charged, the positive ions of the magnesium chloride will help facilitate the folding process by screening negative charge repulsions. The solution was then put in a thermal cycler, which heats up the mixture to 80°C and slowly cools to room temperature. Two thermal cycles (60 hour and 108 hour cooling times) were run to test the effects of cooling rate.

Purification and Analysis of Monomers

After the structures were folded in the thermal annealing ramp, they were purified by aragose gel electrophoresis as previously described. Properly folded structures traveled in bright bands, which were manually excised from the gel, imaged by TEM, and used for polymerization. Figure 18 shows the gels that were run for the 6 helix bundle and the flat 18 helix bundle. The blue box in Figure 18 depicts the 7560 base long scaffold and the green box illustrates the folded 6 helix bundle structures with magnesium chloride concentrations ranging from 14 to 28 mM. The red box on the right shows the 8064 base scaffold for the flat 18 helix bundle. The black and purple boxes depict flat 18 helix bundle Design 2 with magnesium chloride concentrations ranging from 12 to 24 mM for thermal ramps of 60 hours and 108 hours respectively. The orange and yellow boxes show flat 18 helix bundle Design 1 with similar magnesium chloride concentrations for 60 hour and 108 hour folding ramps.

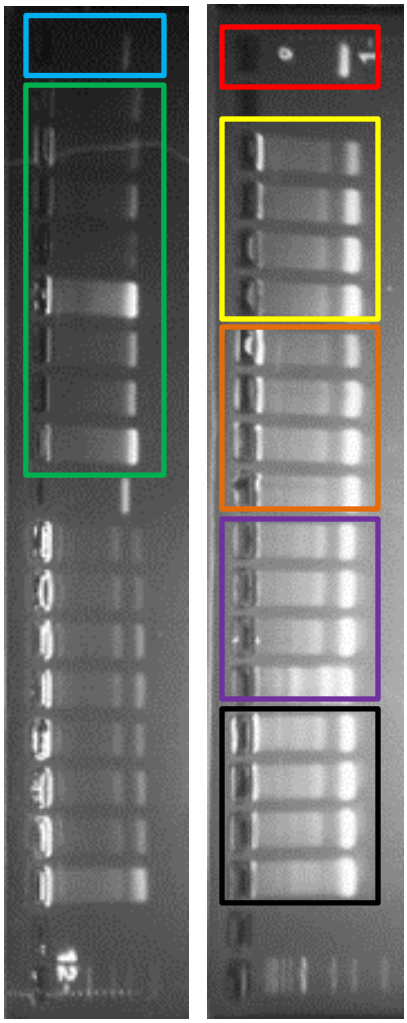

Figure 18: Purification Gel for 6 Helix Bundle (Left) and 18 Helix Bundle (Right)

To image the structures using a TEM, 4 µL of the DNA origami solution was pipetted on to an imaging grid, left for 5 minutes to let the structures settle and adhere to the surface of the grid (Castro, Kilchherr et al. 2011). The excess liquid was then removed through contact with filter paper. Then, 10 µL of 2% uranyl formate, UFo, was added to the imaging grid and incubated for 40 seconds before being removed with filter paper. Figure 20 and Figure 20 are images of 6 helix bundle and flat 18 helix bundle monomers respectively.

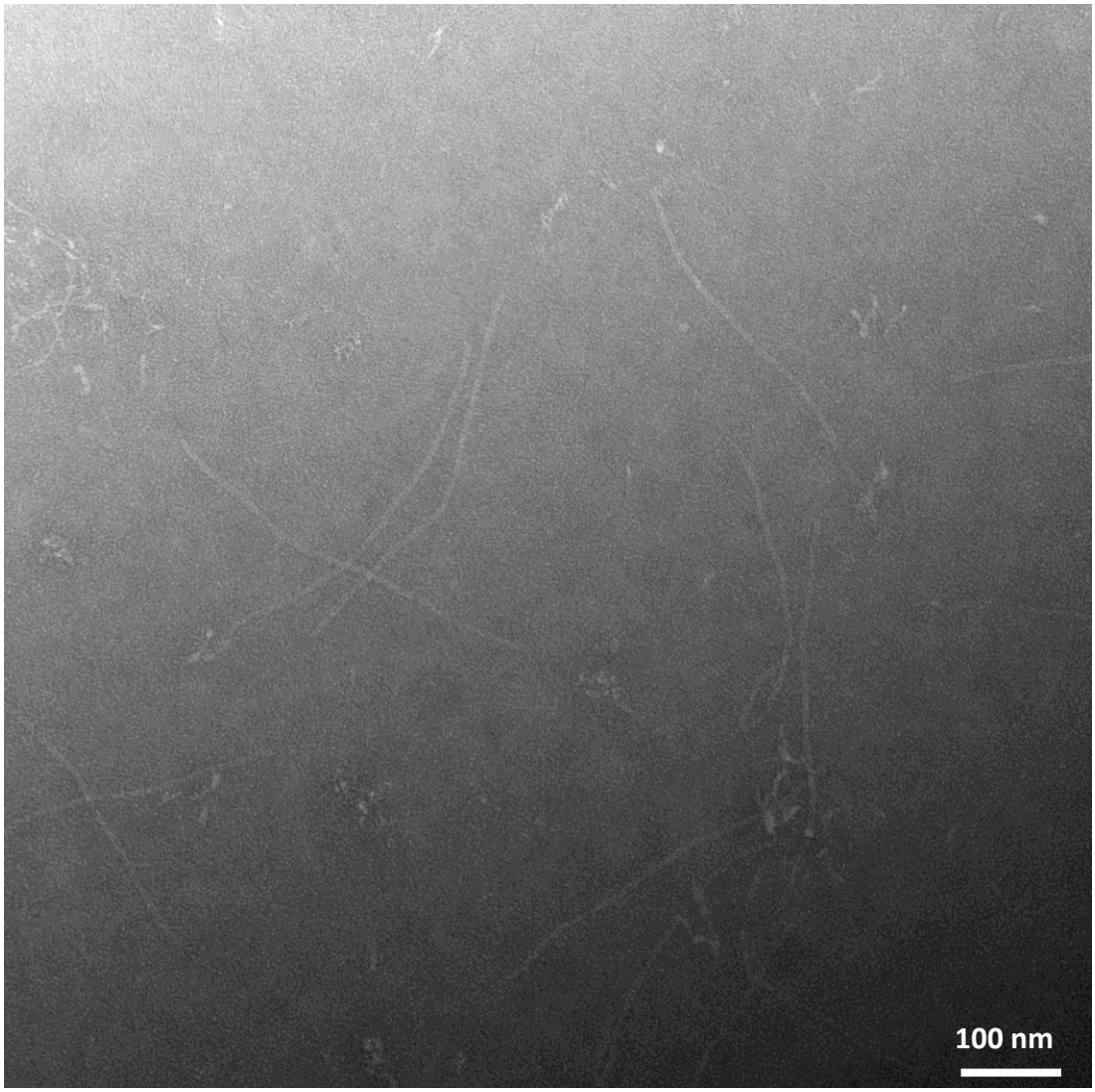

Figure 19: TEM Image of 6 Helix Bundle Monomers

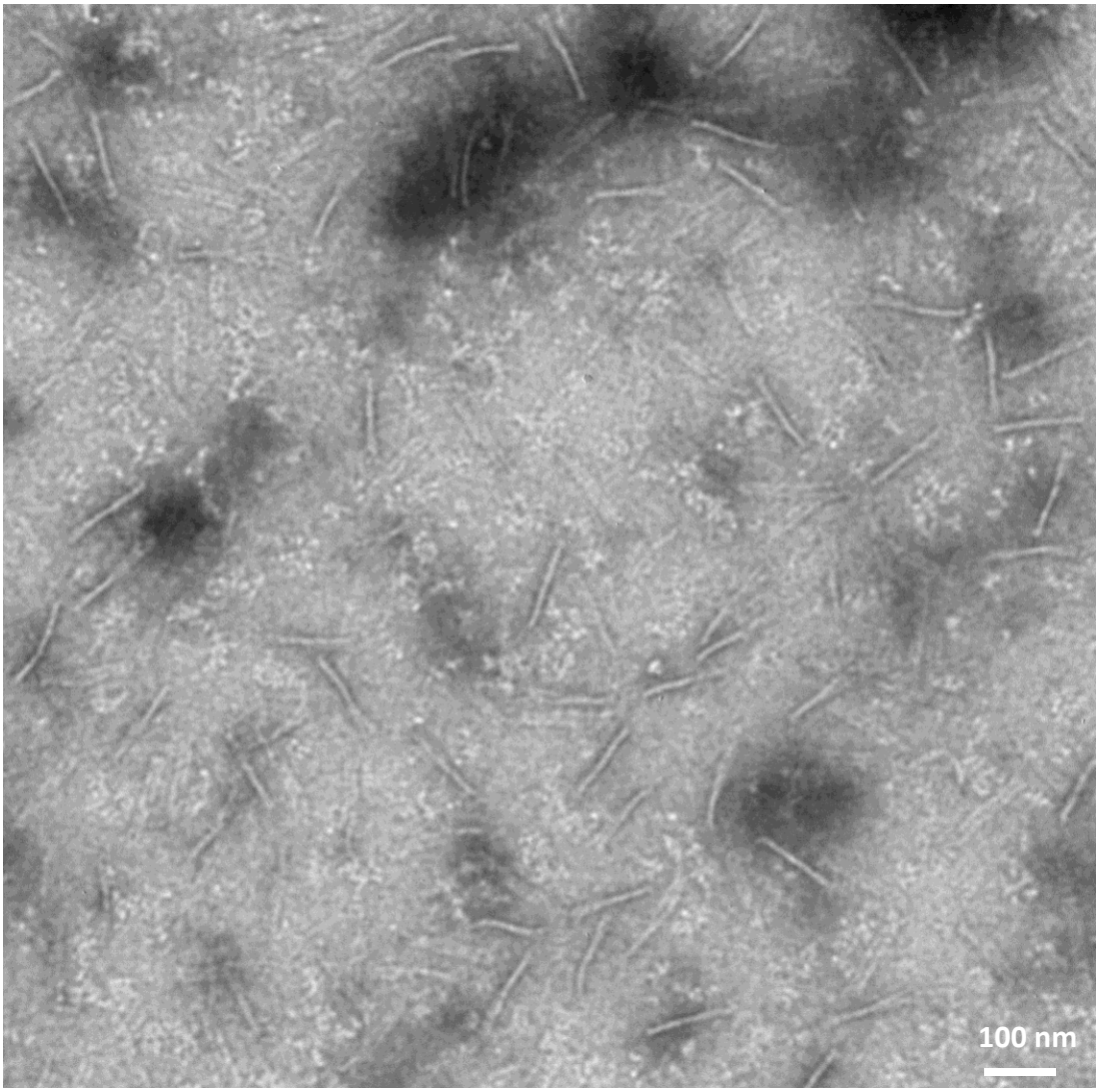

Figure 20: TEM image of Flat 18 Helix Bundle Monomers

Polymerization Reactions

The purified structures were then mixed with the staples designed for polymerization. The new solution of monomers with staples was heated up to 40°C for 24 hours. At the 3, 6, 9 and 24 hour marks of the polymerization, 4 µL of solution was removed from the solution and directly pipetted on to a TEM grid for imaging.

Imaging of Filaments

The DNA origami filaments were prepped for TEM imaging as described by Castro et al (Castro, Kilchherr et al. 2011) at the time points previously mentioned. The polymerized filaments were then imaged using a FEI Tecnai G2 Bio TWIN TEM at the Campus Microscopy and Imaging Facility (CMIF) at The Ohio State University. Figure 21 shows an example TEM image for the 6 helix bundle design and Figure 22 is an example image of the flat 18 helix bundle design.

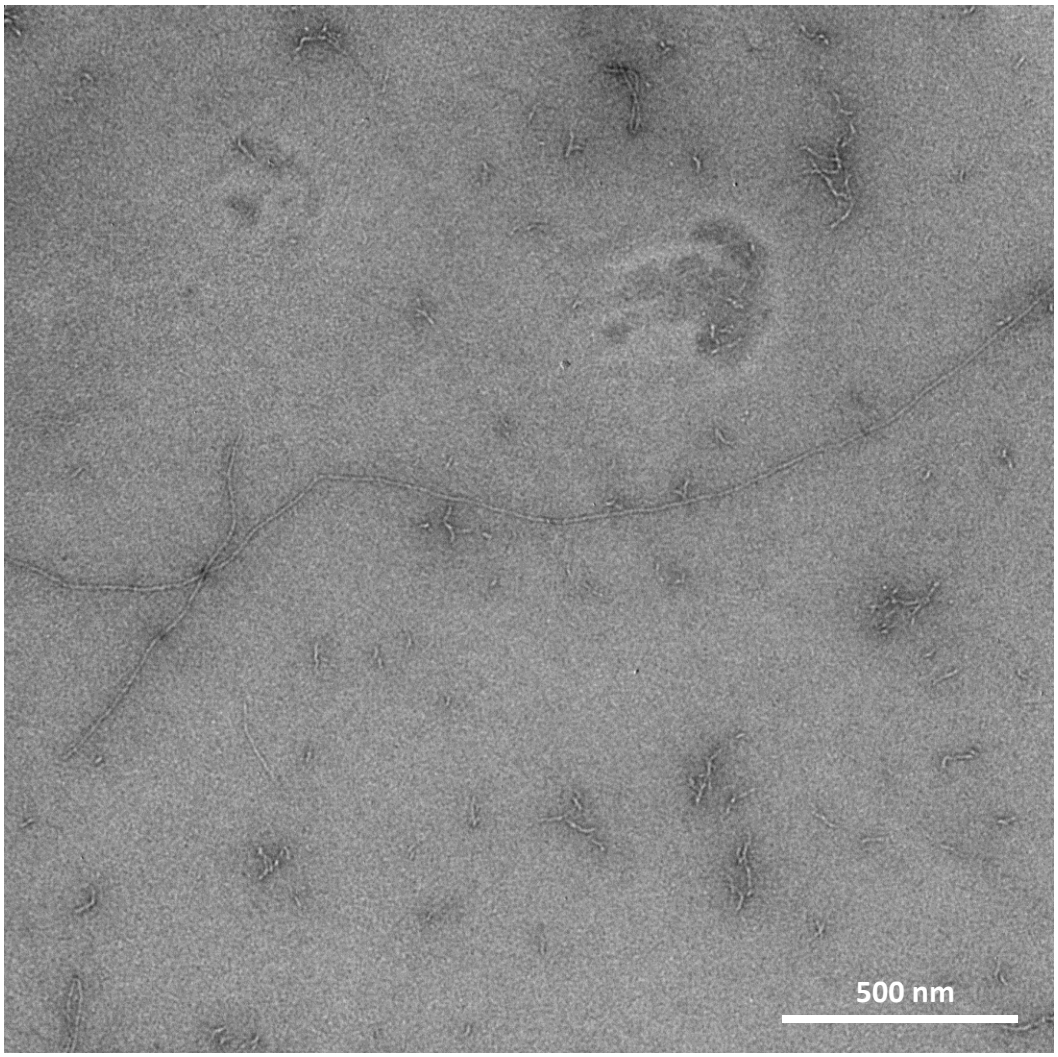

Figure 21: 6 Helix Bundle 24 Hour Polymerization TEM Image

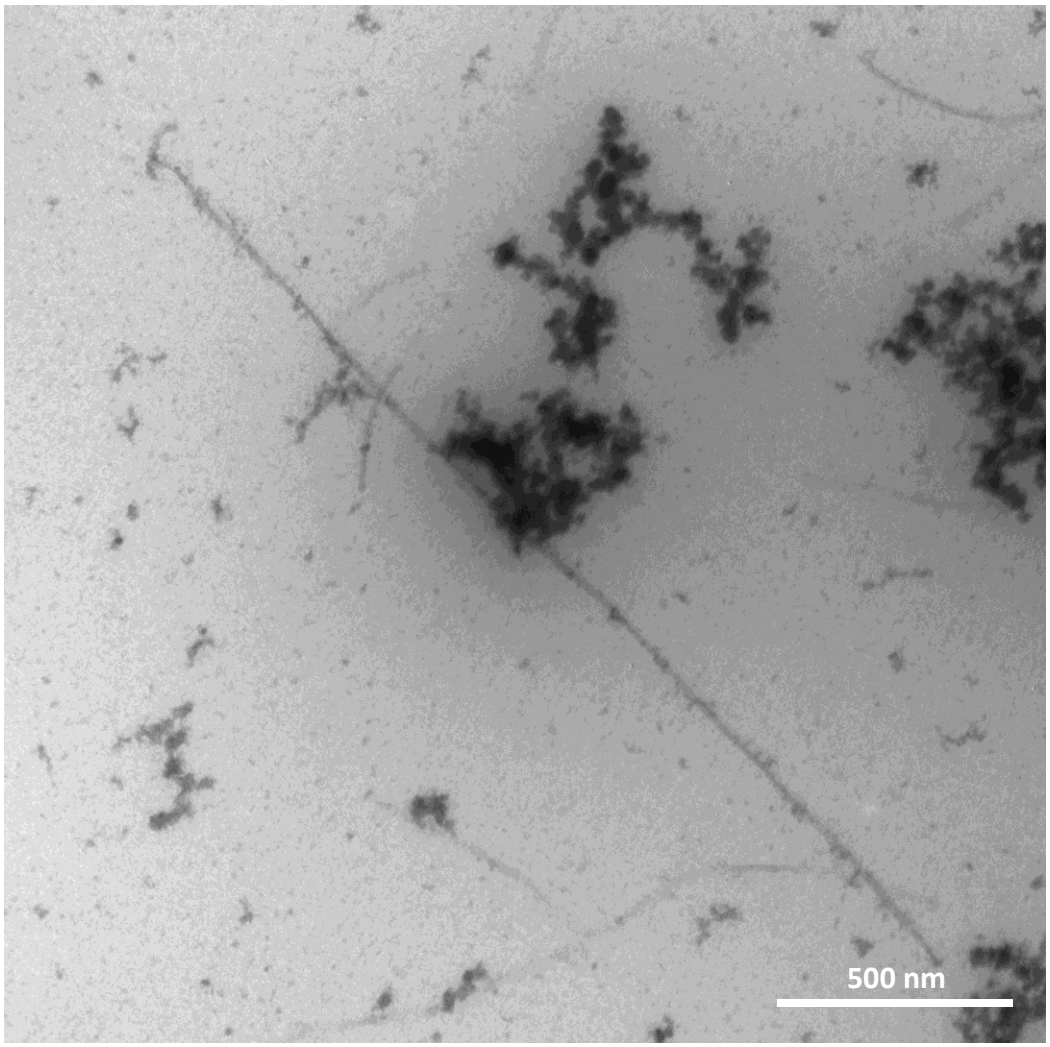

Figure 22: Flat 18 Helix Bundle 24 Hour Polymerization TEM Image

Structure Tracing

To accurately quantify the length of the filaments in the polymerization process, 100 structures were traced from each time point: 3, 6, 9, and 24 hours. Using a Matlab script, points along the length of the structures were manually selected directly on the image. A cubic spline was fit to the selected points and the length of each structure was calculated by summing the individual arc lengths between points. If more than 100 structures were imaged for a given time point, then random numbers were generated and the corresponding structures were omitted from the length calculations. This random selection of structures eliminates bias towards any specific length of structures. Only monomers and filaments that folded and polymerized properly were traced. Figure 23 shows an example of a structure that did not fold properly (ends fold backwards back onto the structure) and was excluded from tracing.

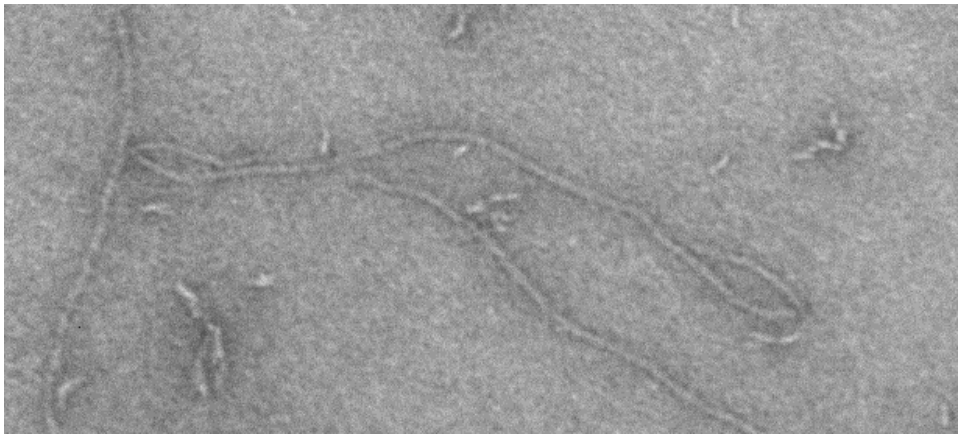

Figure 23: Folding Error of 6 Helix Bundle Structure

Tracing Error

The points that are selected for each filament tracing are selected by hand. Inherently, there is an element of human error associated with the selection of the individual points. To quantify this error, mean, range, and standard deviation were calculated using a sample size of 10 structures for three different length scales: monomers, dimers (2 monomers polymerized together), and trimers (3 monomers polymerized together). Figure 24, Figure 25, and Figure 26 shows the monomer, dimer, and trimer that were traced for error analysis.

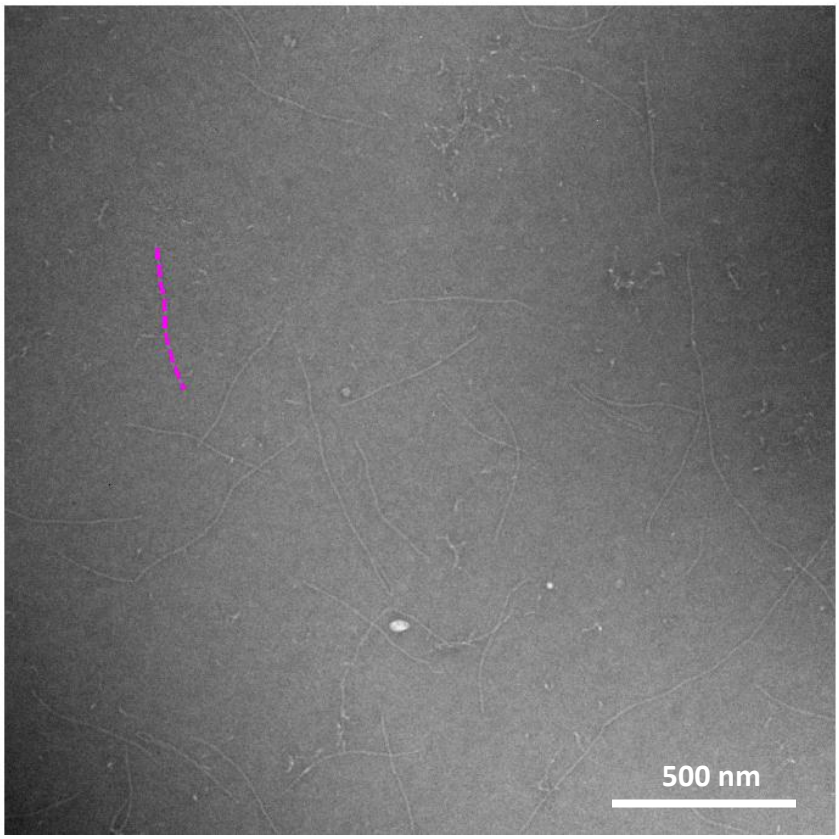

Figure 24: 6 Helix Bundle Monomer Traced for Error Analysis

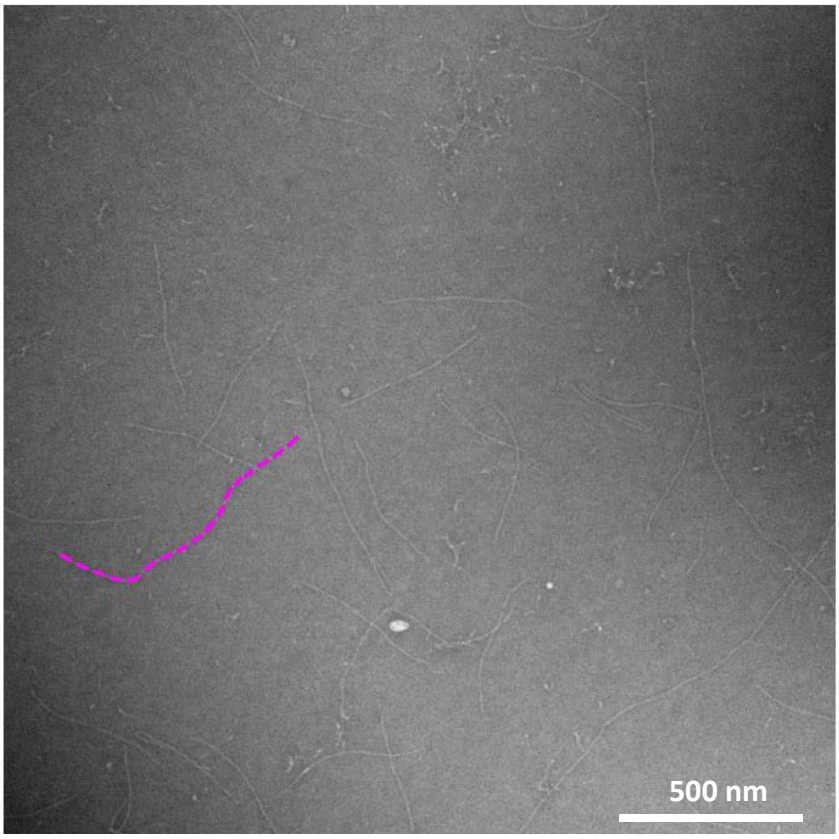

Figure 25: 6 Helix Bundle Dimer Traced for Error Analysis

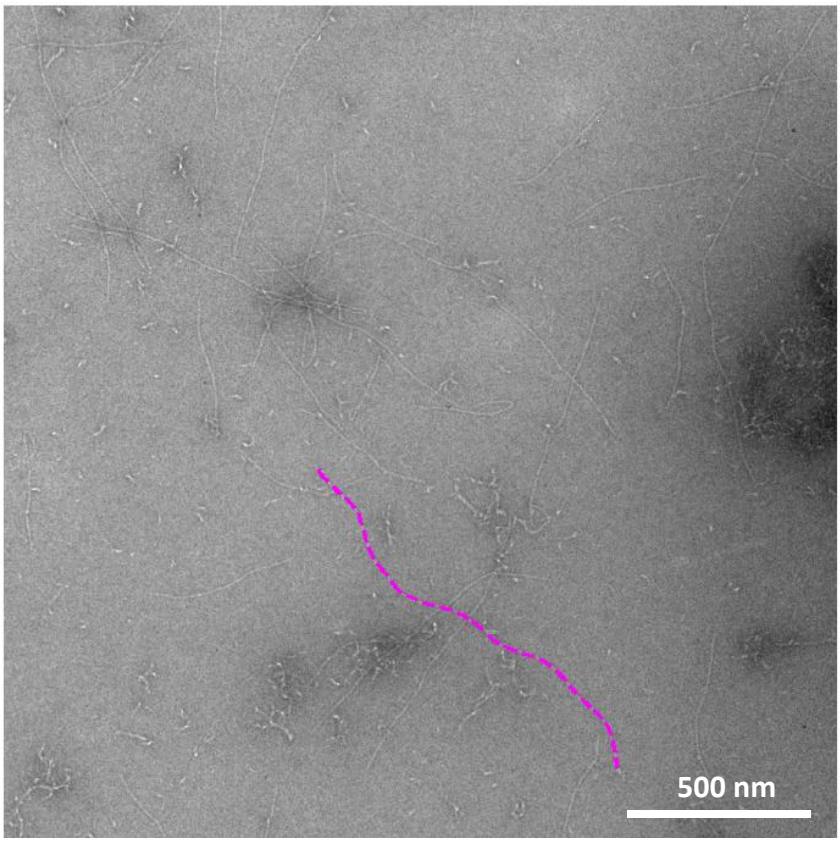

Figure 26: 6 Helix Bundle Trimer Traced for Error Analysis

Table 2 gives the average, standard deviation, range, and theoretical length values for each set of structures that were traced.

Table 2: Statistical Analysis of Structure Tracing for 6 Helix Bundle Design

	6 Helix Bundle Monomer	6 Helix Bundle Dimer	6 Helix Bundle Trimer
Average (nm)	397.37	804.45	1193.58
Standard Deviation (nm)	3.47	3.33	2.85
Range (nm)	13.40	12.51	10.00
Theoretical Length (nm)	401.90	803.80	1205.70

As the structures increase in length, the standard deviation and range of the measurements remains fairly constant. These values verify that the hand tracing method provides an adequate approximation for determining the lengths of the DNA origami structures.

Chapter 4: Experimental Results

6 Helix Bundle Polymerization Results

To assess the filament growth kinetics, the length distributions were compiled for different time points. Figure 27 shows histograms of 6 helix bundle filament length for 3 hour (red), 6 hour (blue), 9 hour (green), and 24 hour (black) polymerization reactions. After 3 hours, the sample still primarily contains monomers. The bins were arranged to increments of monomers, that is from left to right the bins correspond to monomers, dimers, trimers, etc. As the polymerization progresses, the fraction of monomers decreases and the length distributions shift towards the larger filaments.

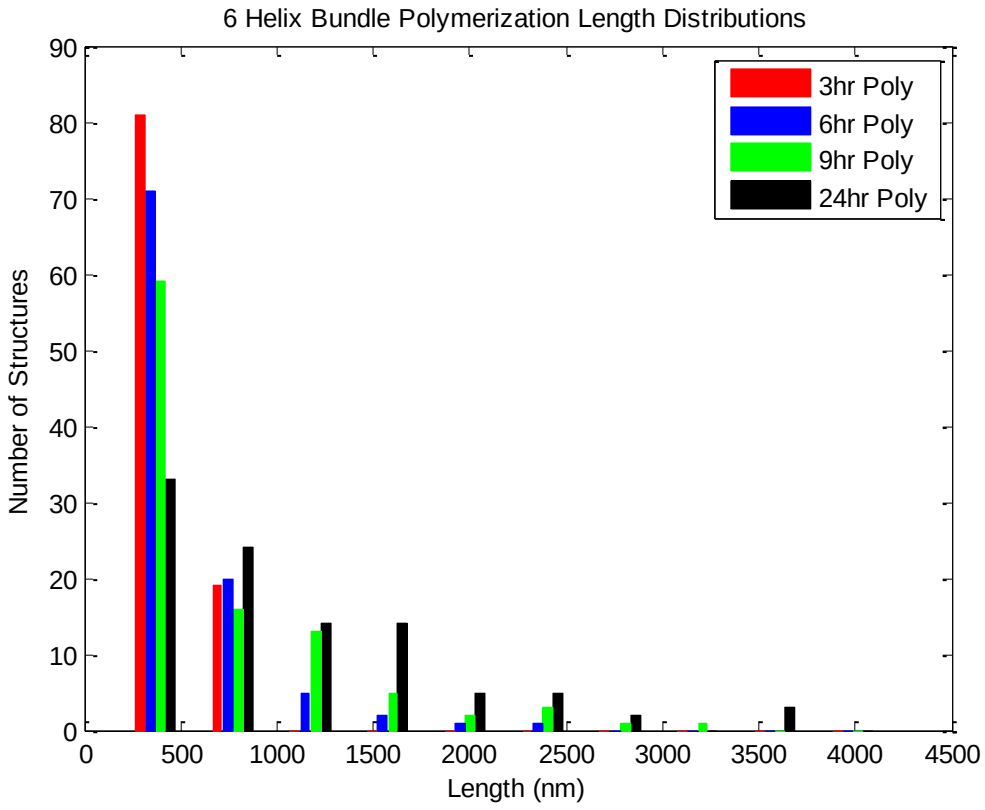

Figure 27: 6 Helix Bundle Polymerization Length Distributions for 3, 6, 9, and 24 Hour Polymerizations

Figure 28 through Figure 31 depict the filament shapes that were completed at each time point during the polymerization process. All of the shape trajectories were aligned so that they start at the same point and initially point in the same direction. These trajectories illustrate the decrease in fraction of monomers as the time increases. Furthermore, these filament trajectory ensembles suggest that the length does not affect the mechanical properties since the ensemble shape doesn't not noticeably change as the filament length increases. While we do not expect the length to affect the mechanical properties, some experimental artifacts due to the surface deposition process may be length dependent, so it is useful to confirm that the length does not largely affect the bending stiffness.

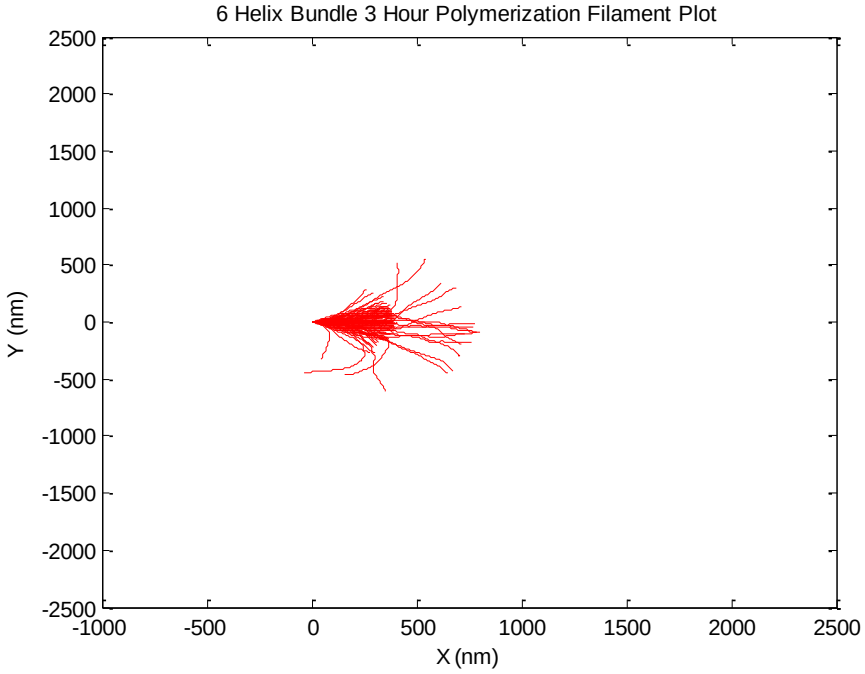

Figure 28: 6 Helix Bundle 3 Hour Polymerization Filament Tracing Plot

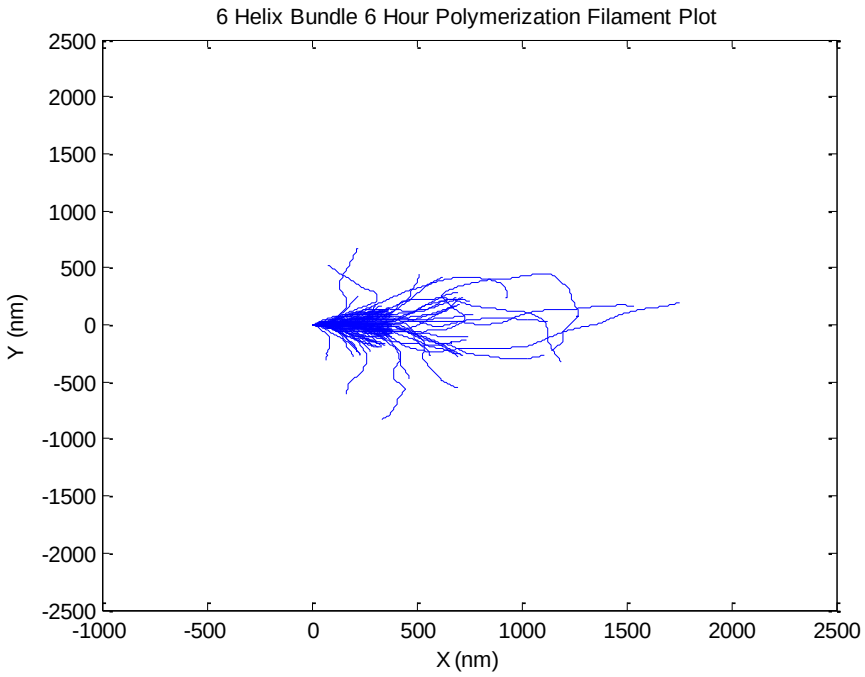

Figure 29: 6 Helix Bundle 6 Hour Polymerization Filament Tracing Plot

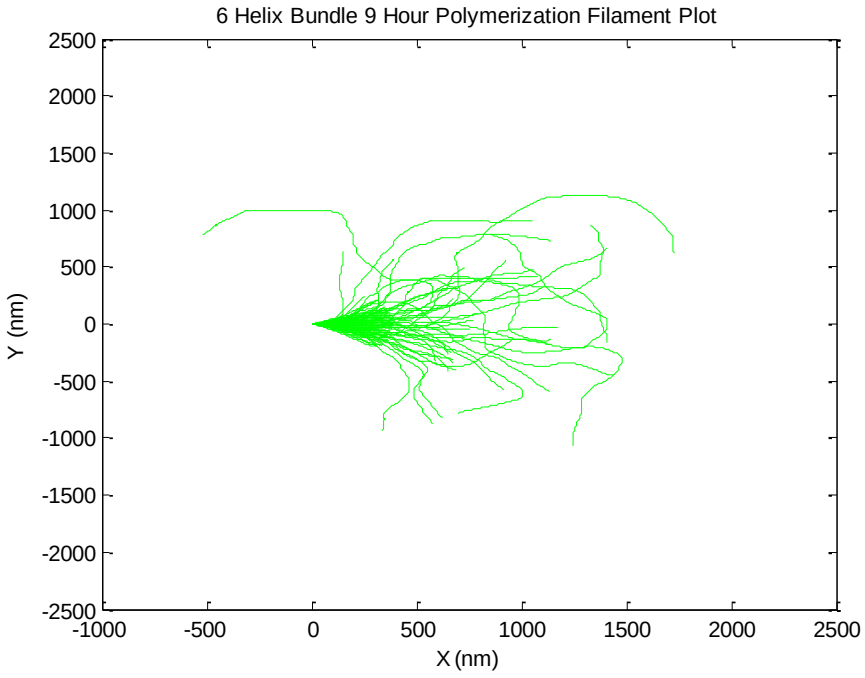

Figure 30: 6 Helix Bundle 9 Hour Polymerization Filament Tracing Plot

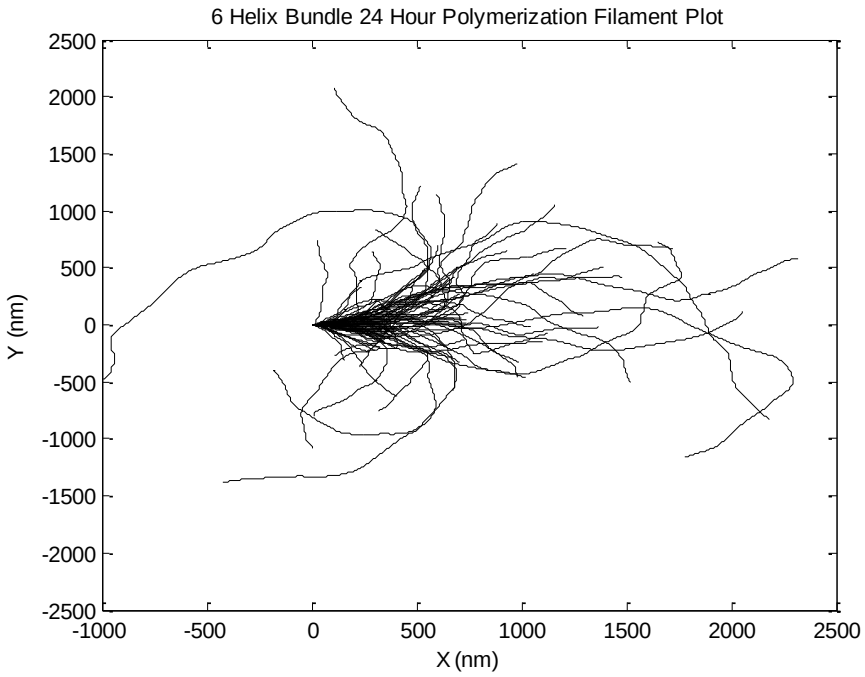

Figure 31: 6 Helix Bundle 24 Hour Polymerization Filament Tracing Plot

Figure 32 shows a plot of percentage monomer in solution and average length of filaments vs. time of polymerization. The percentage monomer value is the fraction of monomers that remain in solution that have not been polymerized. As shown is the curve the percentage monomer decreases as the filament length increases. Our results show that the monomers are largely, but not completely depleted after 24 hours. While the monomers are not completely depleted, the low concentration in solution likely drastically slows down the polymerization process. Further experiments at additional time points would be required to fully characterize the polymerization kinetics.

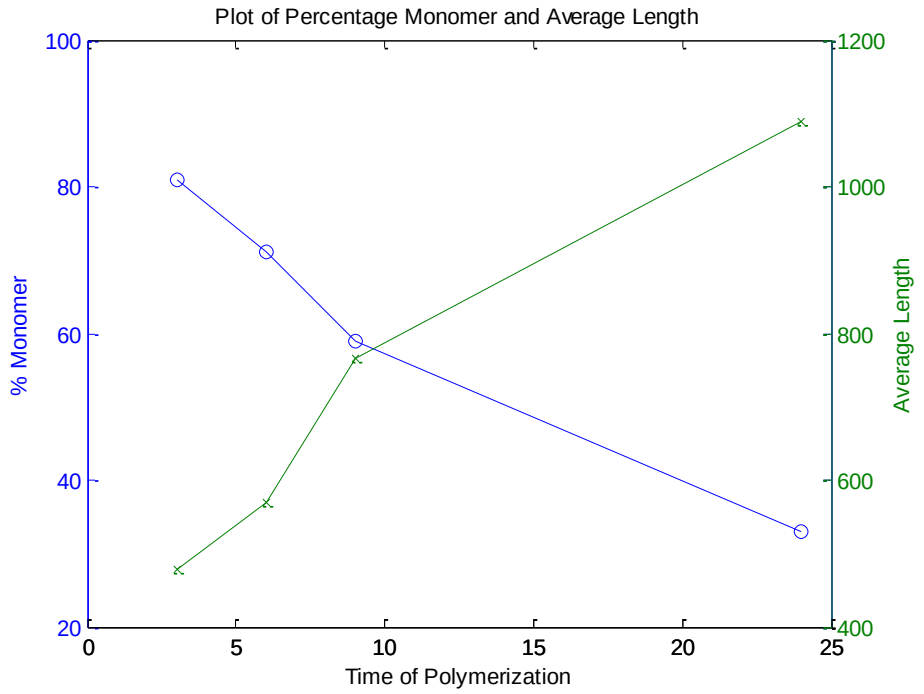

Figure 32: Plot of Percentage Monomer of 6 Helix Bundle structures and Average Length as a Function of Time of Polymerization

The traced filaments can be divided up into categories with respect to the number of monomers in the filament. Quantities of each set are located in Table 3 and grouped by time of polymerization.

Table 3: Count of 6 Helix Bundle Filaments at Different Points during the Polymerization Process

	Polymerization Time			
	3 Hour	**6 Hour**	**9 Hour**	**24 Hour**
# Monomers	81	71	59	33
# Dimers	19	20	16	24
# Trimers	0	5	13	14
# Tetramers	0	2	5	14
# Pentamers	0	1	2	5
# Hexamers	0	1	5	10
Total	100	100	100	100

Figure 33 and Figure 34 show a comparison between the flat 18 helix bundle and 6 helix bundle for a 6 hour polymerization. It takes three flat 18 helix bundle monomers polymerized together to reach the length of a single monomer for the 6 helix bundle. The flat 18 helix bundle filaments look stiffer due to the straighter orientation of the filaments. After a 6 hour polymerization, the average length of the flat 18 helix bundle filament is 279.2 nm and the average filament length of the 6 helix bundle is 569.2 nm. For the flat 18 helix bundle, the average structure is around 2.12 monomers in length where the 6 helix bundle average filament would be around 1.42 monomers in length.

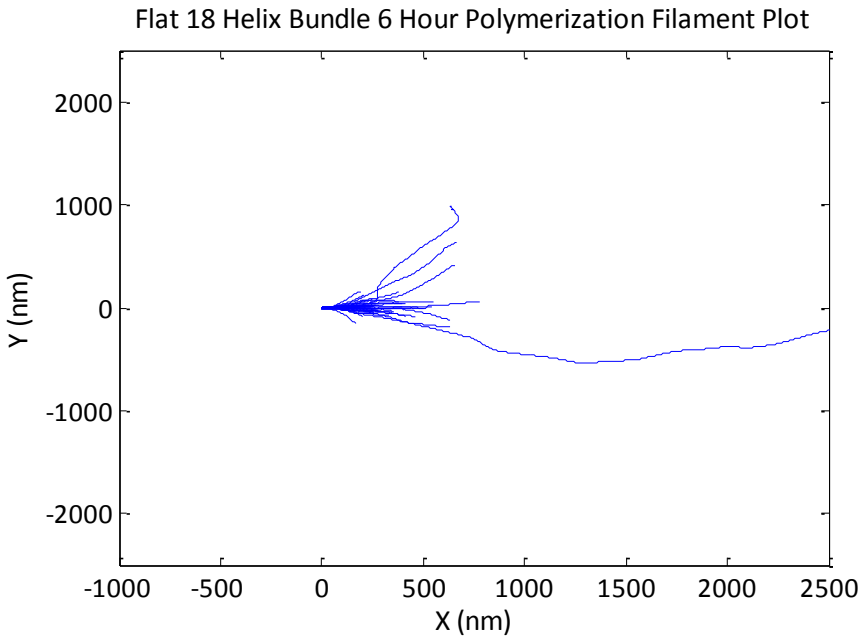

Figure 33: Flat 18 Helix Bundle 6 Hour Polymerization Filament Tracing Plot

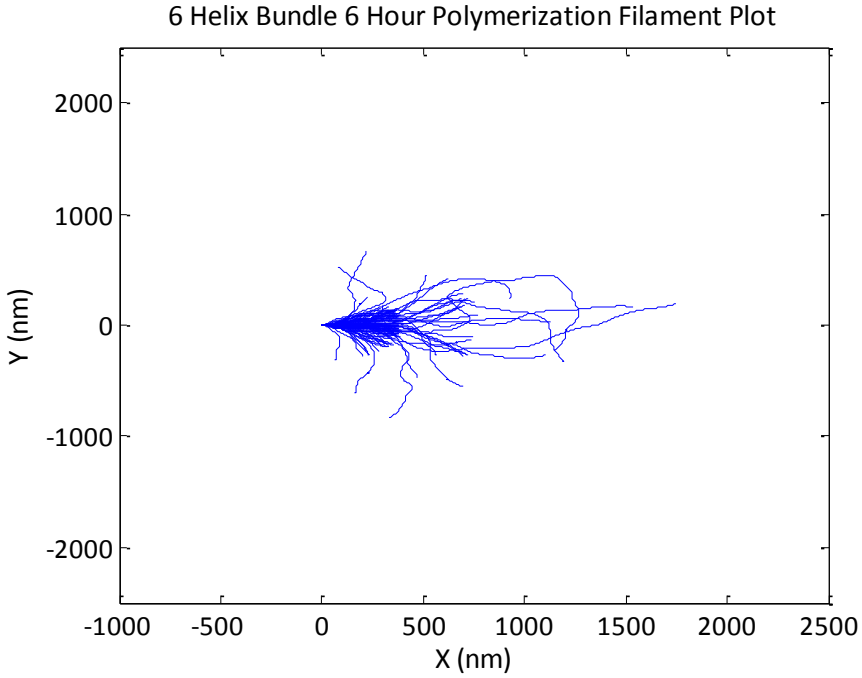

Figure 34: 6 Helix Bundle 6 Hour Polymerization Filament Tracing Plot

Chapter 5: Conclusions and Future Work

Conclusions

The experimental data verifies that the polymerization method is a time dependent process; as the time of polymerization increases, the average length of the filaments increase. Our results also suggest that the growth rate is proportional to the number of monomers in solution. Monomers are the individual building blocks of the filaments. As seen in Figure 32, as the average length of the filaments increase, the percentage of monomers that are left in solution decreases. The less monomers that are in solution, the rate at which the filaments grow should decrease since the monomers will have to diffuse over a larger distance in order to find a filament. This also illustrates that the growth rate and final filament length is highly sensitive to the initial concentration of monomers. Theoretically, if the number of monomers in solution increases, the filaments could continue to increase in length over longer polymerization intervals. In practice, this could be achieved by introducing additional monomers into solution after some time. Figure 32 suggests that introducing additional monomers after 24 hours would enable longer filaments.

The flat 18 helix bundle has been designed and monomers have been folded. The polymerized structures have been imaged using the TEM and the images are ready for analysis. The structures appear to have a high concentration in solution and through a preliminary analysis; the filaments seem to grow at a faster rate than the 6 helix bundle. The mechanical stiffness of the flat 18 helix bundle is also larger compared to the 6 helix bundle.

Future Work

Transmission electron microscopy provides a high resolution medium for imaging DNA origami structures. As discussed, we used TEM to image filaments at different time points to identify the growth rates. We will additionally take time points in the 9 to 24 hour range (12 hour, 15 hour, and 18 hour) to better quantify the filament growth kinetics. In order to fully quantify the growth process, it would be desirable to be able to image filament growth in real time. TEM uses a negative staining procedure that creates a static, two dimensional snapshot of structures deposited on a surface that can be imaged. This process does not allow for the ability to view the structures in solution during the polymerization process in real time. Furthermore, the filaments may be subjected to some force during surface deposition that could cause rupture of the filaments.

Fluorescence microscopy is another medium for imaging DNA origami structures that might provide an avenue to view the polymerization process in real time. Intercalating dye can be used to make the DNA structures fluoresce when excited by a specific wavelength laser. The dye molecules intercalate between the bases of the DNA structures and only fluoresce when bound to with double stranded DNA. Initial experiments have been conducted and preliminary results are depicted in Figure 35. For this experiment, structures were polymerized for 24 hours and then a sample was prepared for fluorescence imaging.

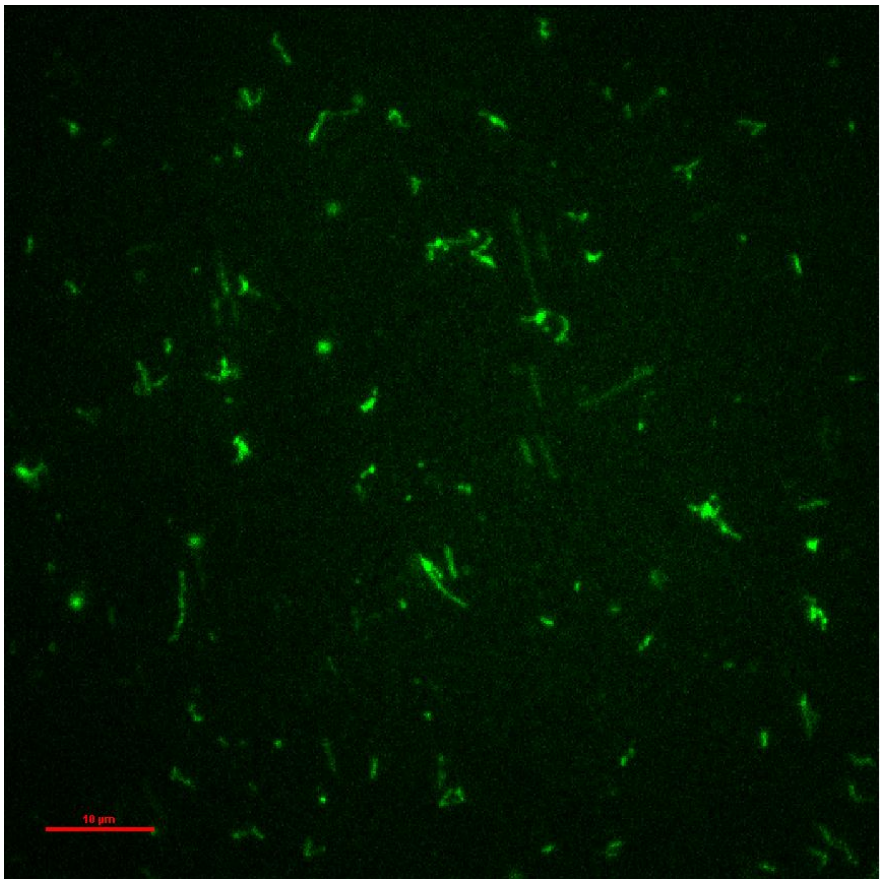

Figure 35: Fluorescence Microscopy Image of Polymerized 6 Helix Bundle

The image resolution of the fluorescence images is lower than the TEM images, but the structures are not fixed by using a negative staining process. With the use of time lapse photography and a microscope stage-top incubator, the polymerization process can theoretically be viewed in real time in a variety of polymerization conditions.

Currently, there is a concern with the photo bleaching of structures under long exposure to the laser which is hindering data collection. One possible solution is to add as anti-photo bleaching agent to the structure to view them periodically over a 24 hour period. Along with the photo bleaching problem, there is a problem with the fluctuation of the structures over the

polymerization period. The filaments move in and out of the image plane of the microscope and it becomes difficult to track the movement. One way to solve this is by adhering one end of some monomers to the bottom of the coverslip so they will stay in the image plane. Monomers that are free in solution will now bond to the monomers that are stuck to the surface, which can be imaged.

The flat 18 helix bundle features various designs that attempt to improve the polymerization parameters of geometric precision and monomer-to-monomer bond strength. Each of the designs will be folded and polymerized to determine if the neighboring staples and the polymerization staple toehold make a difference in the polymerization process. With this data, current monomer designs can be updated with the best possible polymerization staple configuration. One aspect of the flat 18 helix bundle design is that fluorescently labeled staples can be implemented. The large cross sectional area allows for these FRET, fluorescence resonance energy transfer, staples to bond to each end of the monomer. When two monomers bond together, the intensity of the fluorescence can be captured and analyzed to determine the length of the structure. If the small scale experiments work, then they can be scaled up to find the bulk fluorescence with the use of a spectrophotometer, which measures fluorescence in solution.

To address the poor geometric precision of the polymerization process, constraining of the structures in small nanofluidic channels are currently being investigated. The current polymerization process is conducted in solution in 3-D space. Constraining the structures in nanofluidic channels should lock the monomers into the proper orientation to be polymerized. One advantage to the nanochannel implementation is that different staples groups and buffers

can be introduced into the channels during the polymerization process. This work is being done in conjunction with Dr. Prakash's lab at The Ohio State University.

References

Castro, C. E., F. Kilchherr, et al. (2011). "A primer to scaffolded DNA origami." Nat Meth **8**(3): 221-229.

Douglas, S. M., H. Dietz, et al. (2009). "Self-assembly of DNA into nanoscale three-dimensional shapes." Nature **459**(7245): 414-418.

Jungmann, R., M. Scheible, et al. (2011). "DNA origami-based nanoribbons: assembly, length distribution, and twist." Nanotechnology **22**(27).

Langecker, M., V. Arnaut, et al. (2012). "Synthetic Lipid Membrane Channels Formed by Designed DNA Nanostructures." Science **338**.

Nelson, D. L. and M. M. Cox (2008). Principles of Biochemistry. New York, W. H. Freeman and Company.

Rothemund, P. W. K. (2006). "Folding DNA to create nanoscale shapes and patterns." Nature **440**(7082): 297-302.

Turowski, D. (2012). An Investigation of Mechanical Properties of DNA Origami Nanostructures. Mechanical and Aerospace Engineering Department, The Ohio State University.

Zhao, Y.-X., A. Shaw, et al. (2012). "DNA Origami Delivery System for Cancer Therapy with Tunable Release Properties." ACS Nano **6**(10).